String Formation in Sheared Polymer Blends: Coalescence, Breakup, and Finite Size Effects

Kalman B. Migler*

Polymers Division, NIST, 100 Bureau Drive, Gaithersburg, Maryland 20899-8542

(Received 12 May 2000)

We have discovered a droplet-string transition in concentrated polymer blends which occurs when the size of the dispersed droplets becomes comparable to the gap width between the shearing surfaces. The transition is abrupt and proceeds via the coalescence of droplets in a four-stage kinetic process. Once formed, the strings are stable and exhibit pronounced hysteresis. The string state is stabilized by a suppression of the Rayleigh-Tomotika instability due to both finite size effects and to the shear-induced advection of small-amplitude disturbances.

DOI: 10.1103/PhysRevLett.86.1023 PACS numbers: 61.25.Hq, 83.50.Ax, 47.55.Dz, 83.80.Hj

Polymer blends are traditionally used in *macroscopic* applications where the synergetic properties of two immiscible polymers can be exploited, such as in nylon/rubber blends [1]. The length scale of the dispersed phase is typically of order 1 μm whereas the smallest length scale, d, of the part manufactured from the blend is much larger (e.g., a car bumper). There is great current interest in micro and nano length scale technologies in which polymer blends could play an important role, but the physics of processing polymeric emulsions when the droplet size is comparable to a sample dimension is poorly understood. Here we report on several novel phenomena that occur in this regime.

The size and morphology of the dispersed component is determined during material processing and is crucial to the final physical properties; for example, fibers can provide great enhancements in unidirectional strength, sheet structures can possess ultralow permeability and spherical inclusions provide impact resistance [1,2]. The fundamental understanding of the dispersion mechanism comes from the works of Taylor and others who have shown the ratio of the viscous to interfacial stresses on a droplet, i.e., the capillary number (Ca), determines its stability in a shear field [3–6]. For the case considered here of (roughly) equal viscosity between droplet and matrix, there is a critical capillary number $\mathrm{Ca}_c \approx 0.5$; droplets in a shear field with $\mathrm{Ca} < \mathrm{Ca}_c$ will remain stable, whereas those with $\mathrm{Ca} > \mathrm{Ca}_c$ will elongate and break up. Using Taylor's definition $\mathrm{Ca} = \sigma a/\kappa$ where a is the unperturbed droplet radius, σ is the matrix shear stress, and κ the interfacial tension, we can define a length scale for a droplet in a shear field, $a' = \mathrm{Ca}_c \kappa/\sigma$. The situation is more complex in concentrated dispersions where droplet coalescence and breakup occur simultaneously, however a' still defines a length scale for the maximum stable droplet size [7,8]. Stringlike structures have been observed in blends which are thermodynamically near a phase transition point [9–12] and in immiscible viscoelastic systems in complex flow fields [13]. While these studies focus on bulk behavior ($a' \ll d$), a two-dimensional simulation has studied the influence of the walls [14]. In this work, we investigate the limit where a' becomes comparable to and smaller than the gap thickness d. Since $\sigma = \dot{\gamma}\eta$, where $\dot{\gamma}$ is the matrix shear rate and η is the matrix viscosity, we can experimentally vary a' through its dependence on $\dot{\gamma}$.

The shear-induced structures are generated by placing the sample in between two parallel quartz disks and rotating the upper one at a controlled rate. The shear rate is then $\dot{\gamma} = \nu(r)/d$ where $\nu(r)$ is the upper plate velocity at the radial point of measurement r. Stroboscopic optical microscopy is utilized to visualize the structures, and the data are recorded onto videotape for subsequent analysis [15]. The minority component is Polydimethylsiloxane (PDMS), used at a mass ratio of 0.28 which is within the range typically utilized in industrial polymer processing, and the majority component is Polyisobutylene (PIB). Both components are fairly Newtonian (constant viscosity) for the shear rates used here and are nearly matched in viscosity; $\eta_{\mathrm{PDMS}} = (10.0 \pm 0.2)$ Pa s and $\eta_{\mathrm{PIB}} = (11.3 \pm 0.2)$ Pa s at room temperature. The materials are weighed, blended, and loaded into the quartz shear cell.

In Figs. 1(A)–1(D) we show video micrographs of the blend structures as the shear rate is progressively deceased at a fixed gap width ($d = 36$ μm). The procedure is to decrement the shear rate in 20% (or less) intervals and wait for system equilibration (minimum wait time is 2 h). In Fig. 1(A) ($\dot{\gamma} = 6.4\ \mathrm{s}^{-1}$), approximately three layers of droplets exist between the disks (as determined by monitoring the velocity of the droplets in the video image). As the shear rate is decreased, the size of the droplets increases so that in Fig. 1(B) ($\dot{\gamma} = 4.1\ \mathrm{s}^{-1}$), only two layers of droplets fit between the disks; in Fig. 1(C), ($\dot{\gamma} = 2.6\ \mathrm{s}^{-1}$) only one layer fits. We observe the unexpected droplet-string transition upon further decrease of the shear rate. Figure 1(D) at $\dot{\gamma} = 2.4\ \mathrm{s}^{-1}$ shows that the droplets have coalesced into very long strings.

We measure the sharpness of the transition by taking advantage of the linear increase in $\dot{\gamma}$ as a function of r. Thus, 8 h after applying a shear rate known to be near the transition, we quickly translate the objective lens in the radial direction. Subsequently, we seamlessly link together images taken at different radial positions (i.e., different shear rates), as shown in Fig. 1(E). Here, the shear rate is 10% higher at the top of the composite image (closer to the outer

 © 2001 The American Physical Society

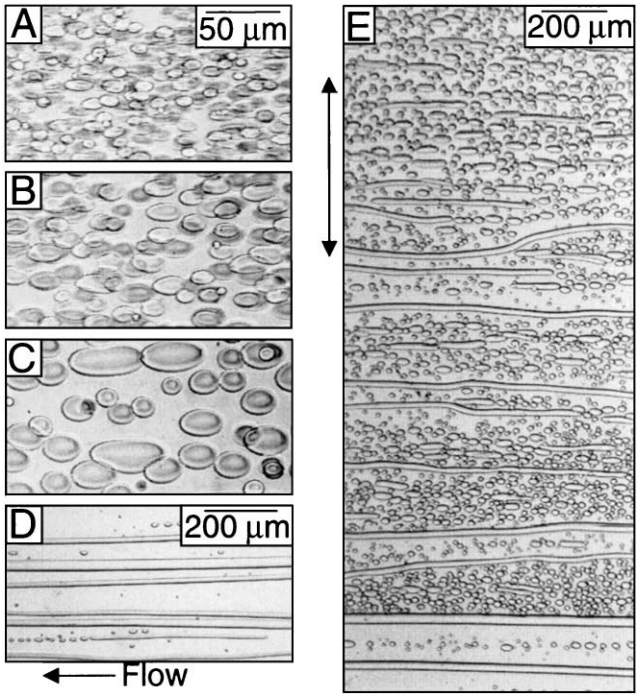

FIG. 1. Droplet-string transition in immiscible sheared polymer blends. Images are in the plane containing the flow (see arrow) and vorticity directions. The distance between the plates in the shear gradient direction (perpendicular to the plane of the image) is $d = 36\ \mu$m. (A) Three layers of droplets at $\dot{\gamma} = 6.4\ \mathrm{s}^{-1}$. For (A)–(D), the distance between the plates in the shear gradient direction (perpendicular to the plane of the image) is $d = 36\ \mu$m; (B) two layers of droplets at $\dot{\gamma} = 4.1\ \mathrm{s}^{-1}$; (C) one layer at $\dot{\gamma} = 2.62\ \mathrm{s}^{-1}$; (D) string transition at $\dot{\gamma} = 2.48\ \mathrm{s}^{-1}$ (note change in scale). (E) In a plate-plate geometry, the shear varies with radial position so that the shear rate at the top is 10% higher than the bottom. The arrow to the left of this composite image shows the width of the transition region. In (E) only, $\eta_d = 30$ Pa s and $d = 40\ \mu$m.

edge) than at the bottom (closer to the center). We observe droplets at higher shear towards the top of the image and strings at lower shear towards the bottom. Over the region of the double arrow, the string length (l_s) over gap width ratio changes from $l_s/d > 25$ to $l_s/d \sim 5$ while the shear rate changes by only 0.025, demonstrating a strong dependence of string length on shear in the transition region.

In order to uncover the relevant scaling laws governing this transition, we carry out a series of measurements as a function of decreasing shear rate for three separate gap widths d ranging from $(36 \pm 5)\ \mu$m to $(122 \pm 5)\ \mu$m. At each shear rate, we measure the size in the vorticity direction of the largest stable droplets l_z. We plot the results as a function of the dimensionless variables l_z/d vs $\dot{\gamma}/\dot{\gamma}_d$, where $\dot{\gamma}_d = \kappa/d\eta$ is the shear rate at which Taylor theory predicts the maximum droplet radius is of order d. Figure 2 demonstrates that the data for the three gap widths collapse onto a universal curve. For all three cases the transition occurs in the vicinity of $l_z/d \approx 0.5$ and $\dot{\gamma}/\dot{\gamma}_d \approx 0.5$. Alternatively, we can

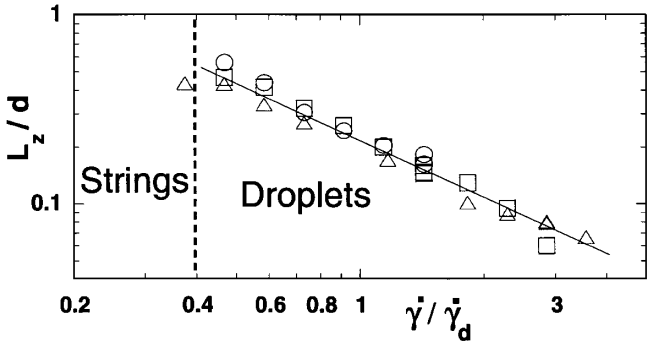

FIG. 2. Scaling of dimensionless droplet width (L_z/d) versus dimensionless shear rate ($\dot{\gamma}/\dot{\gamma}_d$). Experiment was carried out at several values of the gap thickness d: (○) 36 μm; (□) 58 μm; and (△) 122 μm.

decrement the gap width at fixed shear rate. While this procedure is experimentally cumbersome, we do observe the same droplet-string transition. These observations are proof of our central assertion that the transition is governed by the ratio of two length scales; the maximum droplet size to the gap width. This ratio is then determined by $\dot{\gamma}/\dot{\gamma}_d$.

The solid line in Fig. 2 represents a power law with slope -1. The collapse of the data at these reduced shear rates indicates that in the case where the droplets are smaller than the gap ($l_z \ll d$), the droplet size is independent of gap width and scales as $l_z \sim \dot{\gamma}^{-1}$, as expected from the above scaling laws. For the largest gap width of $d = 122\ \mu$m (hence largest droplet sizes), the transition occurs at a slightly lower value of $\dot{\gamma}/\dot{\gamma}_d$. For these large drop sizes, the coalescence rate becomes extremely small, indicating long equilibration times and possible deviations from the -1 power law at $l_z \approx 100\ \mu$m [8,16].

The kinetics of the droplet-string transition upon reduction of shear proceeds in four stages. In the video micrographs of Fig. 3, the shear is reduced from a point just above the transition, $\dot{\gamma}/\dot{\gamma}_d = 0.46$, to a point below it, $\dot{\gamma}/\dot{\gamma}_d = 0.29$. In the first regime, Figs. 3(A) and 3(B), there is an increase in the average droplet size. In the second regime, the large droplets self-organize into pearl necklace structures [Figs. 3(B) and 3(C)]. Eventually, the aligned droplets coalesce with each other to form strings [Fig. 3(D)]. The strings then coalesce with each other [Figs. 3(E) and 3(F)]. The "defect" in Fig. 3(E) (see arrow) shows the mechanism for string-string coalescence. It travels to the left (relative to the midplane velocity) producing a single string of greater width than the individual components. In Fig. 3(F), the middle string width is 150 μm whereas $d = 30\ \mu$m so that the strings are ribbonlike. In the rotating disk geometry, the strings are concentric arches about the axis of rotation. In some cases, they actually form into closed ring structures. In summary, this four-stage process transforms droplets with typical volume $\sim(30\ \mu\mathrm{m})^3$ into strings with typical dimensions ($30\ \mu\mathrm{m} \times 125\ \mu\mathrm{m} \times 75{,}000\ \mu\mathrm{m}$), an increase by 4 orders of magnitude.

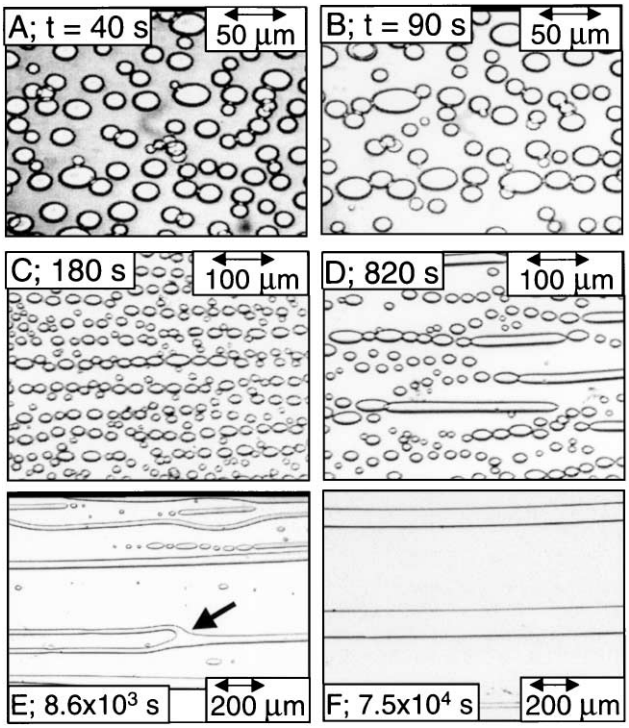

FIG. 3. Kinetics of the droplet-string transition. Shear rate is reduced at t: $t = 0$ s from the droplet regime ($\dot{\gamma} = 4.0\ s^{-1}$) to the string regime $\dot{\gamma} = 2.5\ s^{-1}$. (A)–(B) Increase in size. (B)–(C) Chaining. (D) Coalescence into strings. (E)–(F) String-string coalescence into ribbons.

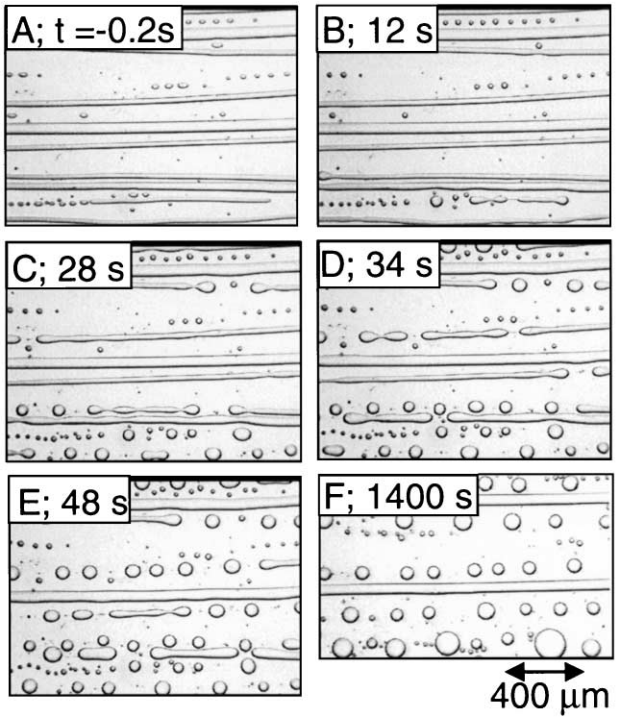

FIG. 4. Suppression of string breakup due to wall-string interactions. For $t < 0$, $\dot{\gamma} = 2.48\ s^{-1}$ whereas for $t > 0$, $\dot{\gamma} = 0$. (A) $t = -0.2$ s; Before cessation, a distribution in width of the strings is observed. (B)–(E) Progressively wider strings break up. (F) Widest two strings are stable (note jump in time).

A key step in the kinetics of the transformation from dispersed droplets to strings is the transient pearl necklace structure shown in Fig. 3(C). Chaining of solid particles has been observed in sedimentation [17] and shear flow [18,19], but has not been reported previously when the dispersed phase is a fluid. In the case of shear and sedimentation, chaining is observed only when the suspending fluid is viscoelastic, i.e., it generates large normal forces under shear. It was shown that the strong viscosity redistributions that occur for a sphere moving in a non-Newtonian fluid relative to a Newtoninan one cause an attractive interaction between spheres that can cause them to line up. In our case, both fluids are Newtonian, and clearly there is no attractive interaction when the droplets are much smaller than the gap width. We speculate that the walls distort the velocity fields when the droplet size is comparable to the wall dimension enough to cause an attractive interaction.

What accounts for the stability of the string structures? Typically, droplets with Ca $\gg 1$ deform and break up, but here they are stable. We propose two distinct mechanisms to explain this phenomenon; the first stability mechanism is due to the walls themselves. The wall induced stability is clearly seen in Fig. 4, which shows the kinetics of the string morphology following the cessation of shear. Figure 4(A) shows that 0.2 s before shear is stopped; there is a distribution of string widths. After cessation of shear, increasingly wider strings break up into droplets [Figs. 4(B)–4(E)]. However, the widest two strings are stable; note the time jump from Fig. 4(E) ($t = 48$ s) to Fig. 4(F) ($t = 1400$ s). From this sequence of micrographs, we find that $l_z/d = 1.2 \pm 0.2$ is the critical ratio marking the transition from breakup to stability upon cessation of flow. Thus the wide stationary strings whose cross sections are large enough that they interact with the walls are stable. In the absence of the wall, they would break up by the Rayleigh-Tomotika mechanism. The wall induced stability of the wide strings stems from a simple dimensionality argument. In three dimensions, a cylinder of radius R is hydrodynamically unstable with respect to an axial fluctuation whose wavelength is greater than $2\pi R$ because it causes a net *decrease* in surface area [20]. Hydrodynamically, the Laplace pressure induces flow from the neck regions where curvature is higher into the bulges where it is lower. In the two-dimensional limit, however, a ribbon is *stable* with respect to an analogous fluctuation because it causes an *increase* in surface area [21] and no change in curvature (i.e., Laplace pressure) from the crest of a fluctuation to its valley. In our system, for the wide strings, the confining walls make the system quasi two-dimensional; fluctuations in the z direction are not allowed. Thermal fluctuations in the y direction are then suppressed because they cause an increase in surface area.

However, the narrower stings in Fig. 4 are stable in the shear field and break up only upon cessation of flow.

A second mechanism that causes strings to be stable was found theoretically by Frischknecht [12], in which a linear stability analysis showed that the Rayleigh-Tomotika instability can be suppressed by a shear field. Varicose fluctuations from one side of the cylinder are convected relative to the other and do not have time to grow. One can define a critical radius for the string: $R_c = \mathrm{Ca}_c^s \kappa/\sigma$ where $\mathrm{Ca}_c^s \approx 0.17$ (for equal viscosity ratio) is a critical capillary number pertaining to strings. The strings are *stabilized* by shear whereas droplets are *destabilized*. Further support for the shear-induced suppression of fluctuations [12] in strings comes from the pronounced hysteresis in the strings. As seen in Figs. 3(E), 3(F), and 4(A), there can be a distribution of string widths. If we subsequently increase the shear rate to $\dot{\gamma}/\dot{\gamma}_d \approx 3$, the strings remain. A further increase to $\dot{\gamma}/\dot{\gamma}_d \approx 20$ makes the narrower ones break up into droplets, but some remain. Beyond that shear rate, instabilities in the matrix are observed (such as voids and instabilities at the outer edge of the plate) due to the high shear rate, and measurements cannot be made. Thus, while the strings are formed by reducing the shear, they are then stable in the high shear regime, defined as $\dot{\gamma}/\dot{\gamma}_d \geq 2$. Strings in the high shear limit can be fairly narrow in cross section, $l_z/d \approx 0.1$, and thus are not interacting with the walls.

Finally, we note that we have observed the droplet-string transition over a range of viscosity ratios from 0.1 to 10, as well as in the case where the matrix is highly elastic, indicating that this phenomenon is generic. To summarize the novel features of this work, we have found a transition from a dispersed state to a string state upon decrease of shear. We have also found that the Rayleigh-Tomotika breakup is suppressed by both finite size effects (in the case of the wider strings) and by shear flow (for the narrower strings). A transient stage in the kinetics of the transformation is the pearl necklace pattern, which has not been observed previously for liquid/liquid dispersions.

One can speculate on applications of these structures—by increasing the viscosity, the size scale should decrease, so that much smaller scale structures can be produced compared to the present experiments. If the string component were conductive and the matrix were an insulator with good mechanical properties, then one could produce wires. If the processing were done at elevated temperature and the string component formed into a fiber, one could have ultrathin materials of high one-dimensional strength. A third application would be to dissolve out the string component and use the resulting structures as scaffolds.

We acknowledge the assistance of Dr. Charles C. Han and A. Frischknecht.

*Email address: kalman.migler@nist.gov

[1] I. Manas-Zloczower and Z. Tadmor, *Mixing and Compounding of Polymers: Theory and Practice* (Hanser Publishers, Munich, 1994).
[2] U. Sundararaj, Y. Dori, and C. W. Macosko, Polymer **36**, 1957 (1995).
[3] G. I. Taylor, Proc. R. Soc. London A **138**, 41 (1932).
[4] G. I. Taylor, Proc. R. Soc. London A **146**, 501 (1934).
[5] B. J. Bentley and L. G. Leal, J. Fluid Mech. **167**, 241 (1986).
[6] H. P. Grace, Chem. Eng. Commun. **14**, 225 (1982).
[7] N. Grizzuti and O. Bifulco, Rheol. Acta **36**, 406 (1997).
[8] J. M. H. Janssen and H. E. H. Meijer, Polym. Eng. Sci. **35**, 1766 (1995).
[9] T. Hashimoto *et al.*, Phys. Rev. Lett. **74**, 126 (1995).
[10] S. Kim *et al.*, Macromolecules **30**, 8245 (1997).
[11] N. S. Martys and J. F. Douglas (to be published).
[12] A. Frischknecht, Phys. Rev. E **58**, 3495 (1998).
[13] H. Vanoene, J. Colloid Interface Sci. **40**, 448 (1972).
[14] H. Zhou and C. Pozrikidis, Phys. Fluids A **5**, 311 (1993).
[15] S. Kim, J. W. Yu, and C. C. Han, Rev. Sci. Instrum. **67**, 3940 (1996).
[16] D. Rusu and E. Peuvrel-Disdier, J. Rheol. **43**, 1391 (1999).
[17] D. D. Joseph *et al.*, J. Non-Newton. Fluid Mech. **54**, 45 (1994).
[18] J. Feng and D. D. Joseph, J. Fluid Mech. **324**, 199 (1996).
[19] D. Highgate, Nature (London) **211**, 1390 (1966).
[20] S. Tomotika, Proc. R. Soc. London A **150**, 322 (1935).
[21] M. S. Miguel, M. Grant, and J. D. Gunton, Phys. Rev. A **31**, 1001 (1985).